Theoretical Chemistry Accounts (2023) 142:23
https://doi.org/10.1007/s00214-023-02963-4

CORRESPONDENCE

First-principle investigation of structures and energy properties of $(Pt_3Cu)_n$, $n = 10–11$ nanoclusters

Carlos D. Galindo-Uribe[1] · **Patrizia Calaminici**[1] · **Omar Solorza-Feria**[1]

Received: 11 November 2022 / Accepted: 25 January 2023 / Published online: 8 February 2023

Abstract
A first-principle study of $(Pt_3Cu)_n$ $n = 10–11$ nanoclusters was performed using the linear combination of Gaussian-type orbitals within the auxiliary density functional theory (ADFT) framework. Neutral, anionic and cationic clusters species were studied. To carry on a detailed exploration of the potential energy surface of these systems, Born-Oppenheimer molecular dynamics (BOMD) simulations have been performed. Several dozens of structures were taken along the generated BOMD trajectories as initial geometries for geometry optimizations. Successive geometry optimizations of these systems, in different electron spin multiplicities and without any type of restriction, were computed. The obtained optimized structures have been characterized by frequency analysis calculations. Computed minima structures, harmonic frequencies, average bond lengths, magnetic moments, spin density plots, dissociation energy, ionization potential and electron affinity are reported. The formation of octahedra moieties has been observed in the most stable structures. The findings of the growing pattern of these clusters can serve as guide to search a synthetic route that can yield nanoparticles with desired geometries and high stability.

Keywords ADFT · Metallic clusters · Growth pattern · Geometry

1 Introduction

Transition metal-based nanoparticles have attracted a lot of attention over the years in different areas of science and technology such as catalysis, medicine, sensors, dyes in between others [1]. One of the most important field for the study of these systems is the catalysis area, in which nanoparticles naturally have a great advantage, thanks to their great catalytic area and their reactivity property, that is between an atomic and a bulk system [2]. The development of new transition metal-based catalysts is also critical to the renewable energy technologies that are of vital importance at the ongoing world energy crisis [3, 4].

Among these catalysts, the development of Pt-based alloys nanoparticles is of special importance, because Pt nanoparticles are excellent for the catalysis of different reactions [1]. However, as it is well known, Pt is very expensive and scarce as excellent metal for catalytic purposes. Moreover, even if Pt is the best catalyst for several reactions, the performance of this catalyst is still far from ideal [as for example in the case of oxygen reduction reaction (ORR)] [5]. To overcome these problems, during the last years, Pt has been alloyed with different less heavy transition metals elements, such as Fe, Ni, Co and Cu, which have the advantage of augmenting the catalytic activity of the resulting material and at the same time diminishing the cost of the obtained catalyst. Within this class of compounds, the Pt_3Cu alloy has turned out to be a good catalysts for different reactions. A short reviewing of these reactions could be done considering the following and therein references. Oezaslan et al. have synthesized Pt and Cu nanoparticles of different composition, and they found that the activity of Pt_3Cu is superior to the one of similar size Pt nanoparticles for the ORR [6]. Sun et al. found that with only a Cu precursor change, was possible to synthesize different nanoparticle geometries: (1) octahedra structures using $Cu(acac)_2$ and (2) twinned icosahedra structures using $CuCl_2$ precursors, respectively [7]. The stability of this alloy for catalysis is particularly evident in nanodentritic Pt_3Cu nanoparticles using a TiN support, which have good catalytic activity toward the ORR

✉ Carlos D. Galindo-Uribe
carlosd.galindo@cinvestav.mx

✉ Patrizia Calaminici
pcalamin@cinvestav.mx

[1] Chemistry Department, CINVESTAV, Av. Instituto Politécnico Nacional 2508, Col. San Pedro Zacatenco Del. Gustavo A. Madero, C.P. 07360 Mexico City, Mexico

even after 10,000 voltammetry cycles [8]. Pt_3Cu also is an impressive catalyst for other reactions such as formic acid, methanol and ethanol oxidation reaction [9–12].

Another interesting property found in the Pt_3Cu alloy is that compared to other Pt:Cu alloys compositions this appears to be more stable. It has been observed that sometimes even using different proportions of Pt:Cu precursors in the synthesis this leads to Pt_3Cu nanoparticles [7]. Furthermore, this alloy is more active against ORR that other alloys [13]. All of these examples show the potential of the Pt_3Cu alloy as a tunable, versatile and very stable catalyst for many applications.

However, this versatility also arises some questions which are still unsolved: What is the most stable structure of this type of alloy as the system size grows? Do the structures observed in different experimental works have any connection between them? These questions could eventually be elucidated theoretically by performing an extensive investigation on this type of nanoparticles on the basis of a reliable first-principle-based study.

Despite of the great importance of this alloy for the field of catalysis, we notice that most of the theoretical studies which have been performed focused on small clusters [14–16]. These studies, however, do not offer a comprehensive understanding of the growth pattern of this system in particular, showing little to no information about the properties of this alloy. On the other hand, first-principle-based investigations have demonstrated to be able to provide correct trends that can be extrapolated to the synthesis of new materials. Different aspects of nanoparticle, design and mechanism have been confirmed and elucidated, such as strain effects [17], atomic layers of precious metals for core@shell behavior [18], crystallographic index reactivity [19], among other geometric properties.

In between various theoretical methods density functional theory (DFT)-based studies have been very useful for this purpose. In particular, auxiliary density functional theory (ADFT) [20] has been proven to be a powerful tool to propose new nanoparticle structures and correlate them to their potential activity as novel catalysts. Different examples, such as the ones which will be mentioned below, are nowadays available in the literature.

Cruz-Martinez and collaborators demonstrated that a progressive model construction of specific cluster sizes can help to identify geometric trends that are useful to build larger clusters and to predict effectively the geometry of the synthesized nanoparticles in the laboratory [21]. Flores-Rojas et al. performing a theoretical modeling with a "small" 44 atom cluster and using appropriate predictors for the ORR reaction showed that PtCoNi nanoparticles had good potential as ORR catalysts [22, 23]. On the basis of this theoretical study, PtCoNi nanoparticles were synthesized and demonstrated to possess superior activity than Pt commercial nanoparticles in the ORR. These studies demonstrate the importance of first-principle-based theoretical investigations in the development of new materials for catalysis and that ADFT is a very powerful theoretical approach to be taken into account for this type of research.

In one of our recent previous work, an extended ADFT-based study on $(Pt_3Cu)_n n = 1-9$ clusters trying to answer questions related to the growing behavior of these systems was performed [24]. The obtained results were quite surprising because the found most-stable structures were found with octahedra and twinned octahedra shapes, being the twinned structures, to the best of our knowledge, not yet been found in experiments [24]. In this work octahedra moieties were found in clusters with a composition near 19 atoms, in agreement with the geometric magic number theory. This finding makes us to think that if the system grows toward the next octahedra geometric magic number, it could occur that either the twinned octahedra moieties is conserved or the simple octahedra moieties arise again. As this is not an intuitive result, in this contribution we investigate the growing behavior of the $(Pt_3Cu)_n, n = 10, 11$ clusters. Therefore, the focus of this study is to increase the size of the previous studied $(Pt_3Cu)_n$ clusters up to a system formed with 44 atoms, which corresponds to the $(Pt_3Cu)_{11}$ cluster. To complete the cluster series from 9 to 11 Pt_3Cu units, here we also investigate the $(Pt_3Cu)_{10}$ cluster. Both clusters have an approximate size of more than one nanometer. This study for consistency is performed with the same theoretical method employed in our previous work [24] whose computational details will be given in the following section. Additionally, cationic and anionic species of the $(Pt_3Cu)_n$ $n = 10, 11$ clusters were also studied with the same methodology to understand if any structural variation might occur between the neutral, positive and negative charged species of these nanoparticles.

This manuscript is organized as follows. In Sect. 2, the computational details are given. In Sect. 3, the obtained results are presented and discussed. Finally, in Sect. 4, the conclusions are summarized together with some perspectives.

2 Computational details

For all calculations the Linear Combination of Gaussian-Type Orbitals Auxiliary Density Functional Theory (LCGTO-ADFT) as coded in the deMon2k program [25] has been employed. For the integration of the exchange-correlation functional, an adaptive grid with a tight tolerance of 10^{-8} a.u. was used [26].

The Perdew–Burke–Ernzerhof modified exchange functional, and the Perdew–Burke–Ernzerhof correlation functional (RPBE-PBE) [27, 28] has been used. This combination of exchange and correlation functionals has been

already successfully used for the theoretical investigation of different Pt-based metallic clusters [22]. For the Cu atom, a triple zeta valence polarized basis set optimized for generalized gradient approximation (TZVP-GGA) was used [29] whereas for the Pt atoms a double zeta quasi-relativistic effective core potential from Los Alamos National Laboratory was employed (QECP|LANL2DZ) [30]. The GEN-A2* auxiliary function set was used for all calculations [29]. For the electronic spin density plots, the QECP used for the Pt atom has been replaced with a triple zeta all-electron basis set [31, 32]. The obtained results are plotted using the Visual Molecular Dynamics (VMD) program [33].

Born-Oppenheimer molecular dynamics (BOMD) have been performed to find initial structures for successive structure optimizations that were computed without any constraints. These canonical simulations were carried on at different temperatures (2000 K and 2800 K) and timings (5–20 ps) using a Nosé–Hoover thermostat to maintain the average temperature [34, 35]. Along the trajectories of these simulations, several dozens of structures were extracted for each cluster size and geometry optimizations in different spin multiplicities were then performed without any restriction.

Once optimized, the most stable structures were characterized by frequency analysis, using the analytic second derivatives of the ADFT energy with respect to nuclear displacements at the optimized geometry [36]. The average bond length (ABL) and the approximate size were calculated using an Octave program developed by the authors [24].

3 Results and discussion

3.1 Lowest energy structures, magnetic moments and spin density

In Fig. 1 the four most stable structures found for each studied nanocluster size are depicted. Cu atoms are represented with red spheres and Pt atoms with light gray spheres, respectively. The spin multiplicity and the symmetry point group for each isomer are also indicated in this figure. The most stable structures are labeled with (10a) and (11a), respectively. The relative energy of these lowest energy nanocluster structures with respect to the other found low-lying stable isomers are given in eV.

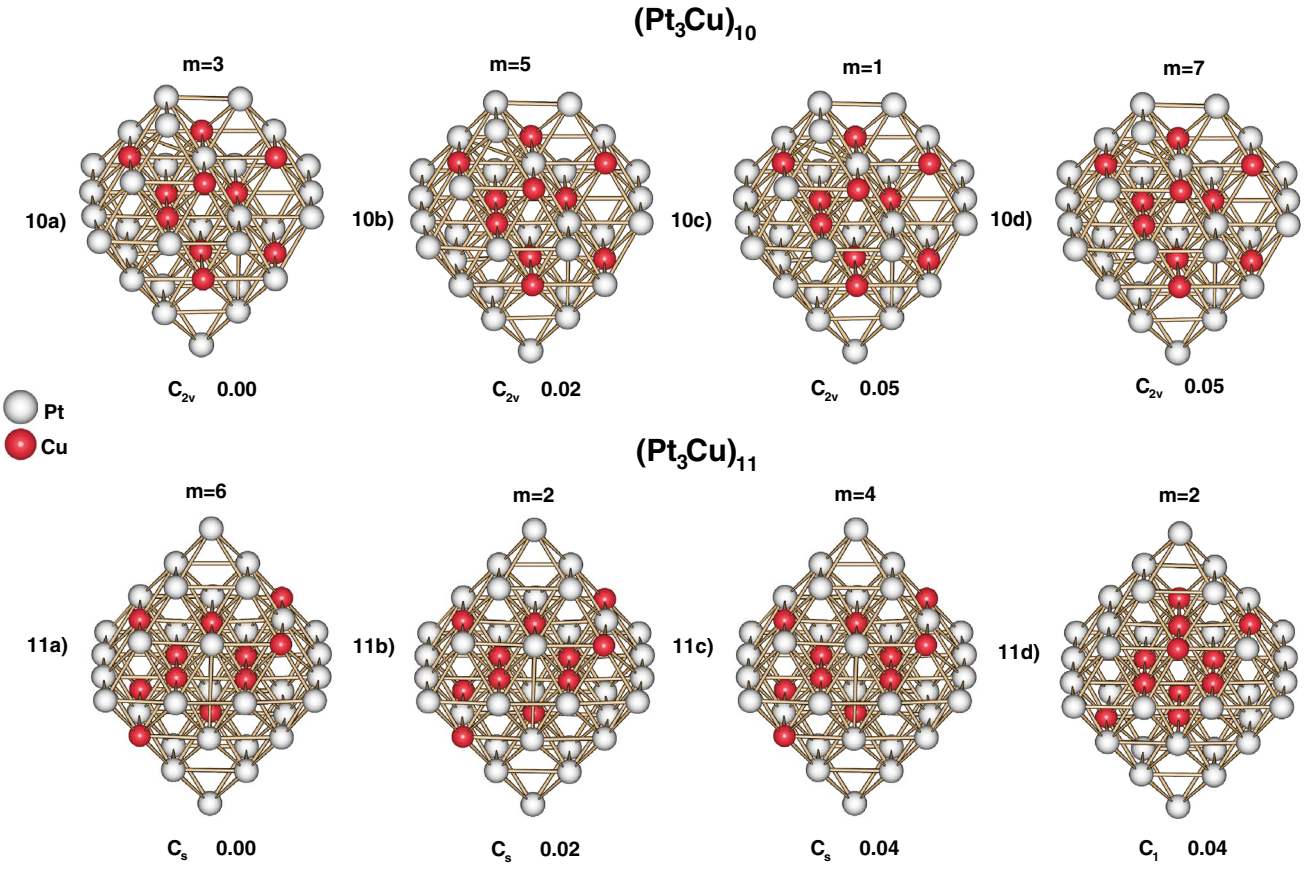

Fig. 1 Structure, spin multiplicity, symmetry point group and relative energy (in eV) of the four most stable isomers of $(Pt_3Cu)_n$ nanoclusters with $n = 10–11$

Turning to the analysis of the obtained results, we focus first on the most stable isomers calculated for the $(Pt_3Cu)_{10}$ cluster, whose structures are graphically displayed in the first row of Fig. 1. Isomer (10a) is found on the triplet PES. The following isomer (10b) has a quintet spin multiplicity and a relative energy of 0.02 eV with respect to the found most stable structure. Isomers (10c) and (10d) have singlet and septet spin multiplicity respectively, are isoenergetic between each other and result to be 0.05 eV less stable than the (10a) isomer. We notice that all most stable isomers of the $(Pt_3Cu)_{10}$ cluster possess a C_{2v} symmetry point group, with very similar structure and atomic distribution. The structure of these isomers can be seen as an octahedron like system which misses atoms at one of the apexes (Fig. 1). This result infers that this atomic like octahedron arrangement could be indeed a very stable structure for this type of clusters. We observe that two Cu atoms are occupying internal positions of the cluster, whereas the rest of these atoms are arranged in two "T" patterns, similar to the cross-type pattern we found in structures of these type of clusters of smaller sizes [24].

The second row of Fig. 1 illustrates the optimized structures of the four most-stable isomers found for the $(Pt_3Cu)_{11}$ nanoclusters. Isomer (11a) presents an octahedron-type structure in the C_s symmetry point group. This isomer is found on the sextet potential energy surface. Isomers (11b) and (11c) present the same structure of isomer (11a), with a spin multiplicity of doublet and quartet and a relative energy of 0.02 and 0.04 eV with respect to structure (11a), respectively. Structure (11d) is also an octahedron like structure but in the C_1 symmetry point group, with doublet spin multiplicity. We notice that this isomer is isoenergetic to the (11c) isomer (see Fig. 1). Interestingly we notice that for the $(Pt_3Cu)_{11}$ cluster all found most stable isomers possess an octahedra-type structure, in agreement with the geometric magic number theory for a 44-atom cluster. Therefore, our calculations underline the fact that the Pt_3Cu clusters grow toward next octahedra magic numbers, instead to conserve twinned octahedra moieties. We also notice that the structure of all most stable isomers obtained for this cluster present Cu atoms occupying six internal positions of the system.

The optimized structures of the $(Pt_3Cu)_n n = 10, 11$ clusters were characterized by analytical frequency analysis calculations. All calculated frequencies are real, indicating that the presented nanoclusters are minima on their respective PES. In Tables 1 and 2 of SI, the calculated normal modes of the lowest energy structures, (10a) and (11a), are listed, respectively. Figure 2 shows the simulated IR spectra of the $(Pt_3Cu)_n n = 10, 11$ clusters. The IR active frequency range goes from about 30 cm^{-1} to about 220 cm^{-1}. We notice that the simulated spectrum of the smaller $(Pt_3Cu)_{10}$ cluster, shown at the top part of Fig. 2, presents more dense peaks than the $(Pt_3Cu)_{11}$ cluster (bottom of Fig. 2). The IR

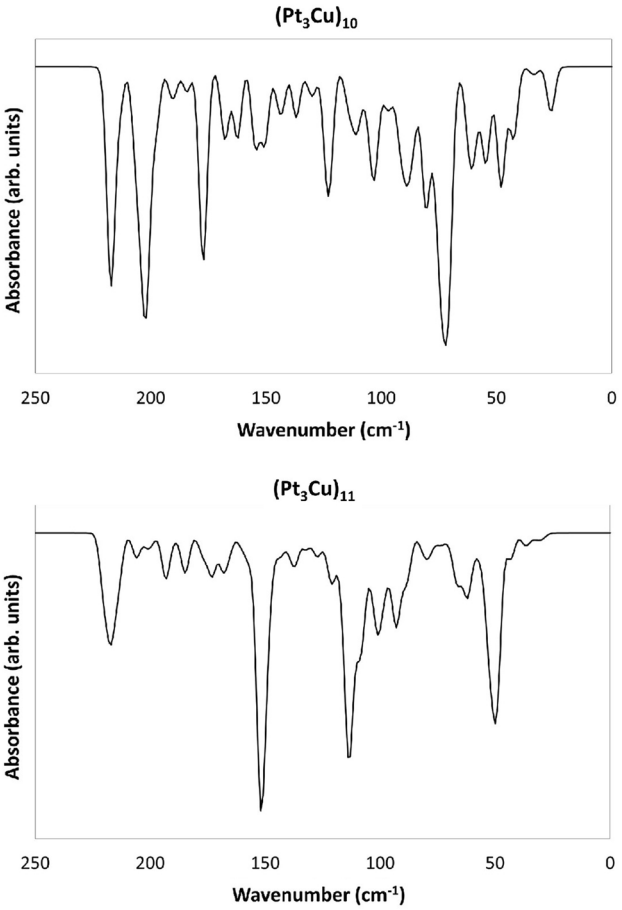

Fig. 2 Simulated IR spectra of the most stable clusters of $(Pt_3Cu)_n$ clusters with $n = 10$–11. See Figure for details

spectrum of the $(Pt_3Cu)_{10}$ cluster shows the greatest absorbance at around 70 cm^{-1}, followed in absorbance by a series of peaks found at around 200 cm^{-1}, 220 cm^{-1} and 170 cm^{-1} (Fig. 2). Concerning the simulated IR spectrum of the $(Pt_3Cu)_{11}$ cluster, the greatest absorbance peaks are, in order of intensity, at 150 cm^{-1}, 115 cm^{-1}, 50 cm^{-1}, and 220 cm^{-1}, respectively. The rest of the active IR peaks of these clusters are in general broader and smaller. The calculated frequencies and the simulated IR spectra could be used as guide in future experimental works to identify potential synthesized Pt_3Cu-based nanoclusters.

In order to get an insight view into the growing pattern of these nanoclusters, in Fig. 3 the most stable structures of the $(Pt_3Cu)_n n = 1 - 9$ clusters [24] are shown along with the most stable $(Pt_3Cu)_n n = 10, 11$ cluster structures from this work. In Fig. 3, the spin multiplicity, the symmetry point group and the approximate size in nm for all cluster structures are also given.

As previously discussed, the analysis of the here obtained stable structures with increasing cluster size shows that the structure of the $(Pt_3Cu)_1$ unit is not

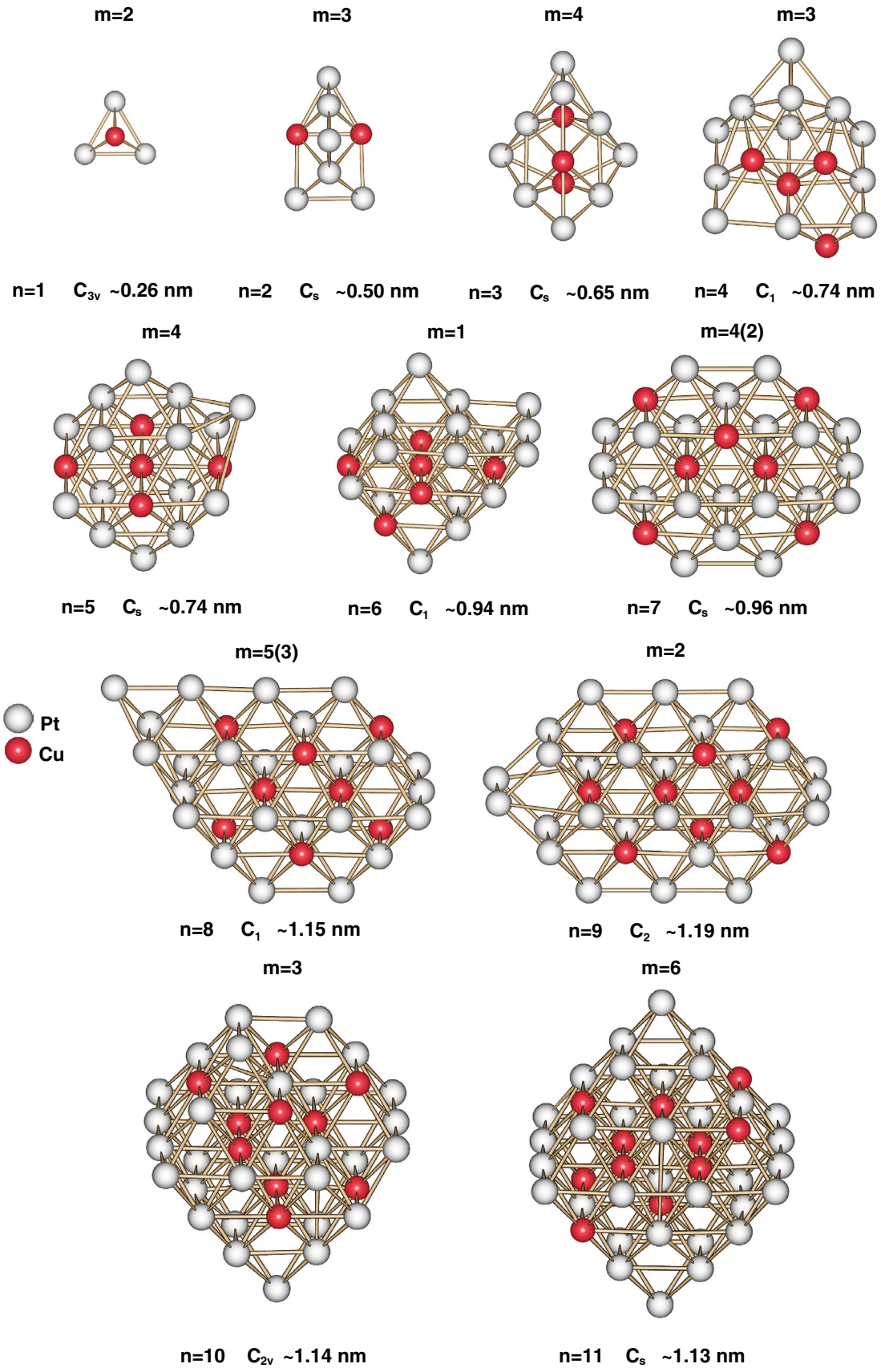

Fig. 3 Most stable structures of $(Pt_3Cu)_n$ nanoclusters with $n = 10–11$, spin multiplicity, symmetry point group and approximate size (in nm)

conserved in the $(Pt_3Cu)_n$ $n = 2–11$ cluster structures. The atomic arrangement found in all cluster structures presents a general tendency of the Cu atoms to occupy internal positions of the system whenever these are available, similar to was previously found in the structures of the $(Pt_3Cu)_n$ $n = 5–11$ clusters [24]. In fact the external Cu atoms in the $(Pt_3Cu)_n$ $n = 5–11$ form also T-shaped and cross-shaped patrons with the central Cu atoms. This particular arrangement in octahedra moieties makes that the Cu atoms prefer to be close together at the same time that the central atomic positions are occupied. This is specially seen in the $(Pt_3Cu)_{11}$ cluster, in which all six internal atoms are Cu atoms. The structure arrangement made by the Cu atoms can also be seen as a 6-atom octahedron Cu core enveloped in a shell of Pt and Cu atoms, confirming our hypothesis from the smaller clusters study [24].

As it can be seen in Fig. 3 the cluster size increases from about 0.25 nm for the smaller cluster (Pt_3Cu) to about more than 1 nm for the $Pt_{33}Cu_{11}$ cluster. To the best of our knowledge this is the first time that nanometric sizes of these type of complex transition metal-based clusters with more than 40 atoms are studied with a first-principle theoretical method.

A very important result of the investigation of this series of Pt_3Cu clusters is the founding of two different (and almost alternating!) moieties in the $(Pt_3Cu)_n$ $n = 4–11$ clusters size range. As we have seen in the previous study, the small $(Pt_3Cu)_4$ cluster presents a square-pyramid fragment with a base of 3×3 atoms. This pyramid can be seen as an incomplete octahedron formed with 19 atoms. This octahedron is completed at the stage of the $(Pt_3Cu)_5$ cluster, and this fragment continues to be present in the $(Pt_3Cu)_6$ cluster. However, in the $(Pt_3Cu)_n$ $n = 6–9$ clusters size range, we notice that the cluster grows in a $\langle 110 \rangle$ direction, forming now "twinned" octahedra-type structures, as found in some minerals, in which a regular crystal grows in one direction. However, as we can see from the results of the present study this tendency of twinning is broken at the cluster size formed with 10 Pt_3Cu units, which similarly to the small $(Pt_3Cu)_4$ cluster, it can be seen as an incomplete octahedron. The octahedron structure is then completed at the stage of the $(Pt_3Cu)_{11}$ cluster. With this picture, is found that this system is governed within the "geometric magic numbers" theory in which 19 and 44 are numbers of atoms which give specially stable structures that can form an octahedron geometry. It is important here to underline that when the number of atoms approaches a magic number the twinning octahedra are no longer the most stable structures, and the single octahedron-type structures becomes more stable. This explains the decrease in the approximate cluster size found between the $(Pt_3Cu)_n$ clusters formed with $n = 9$ and $n = 10$ clusters, as result of the change of the growing direction of the system (see Fig. 3).

To explore the stability of these nanoclusters, the dissociation energy were calculated considering two different types of fragmentation. The classic dissociation energy, denoted here as $D_{0,at}$, was calculated as the ponderated average of energy needed to extract one atom from a cluster. Also, to find the stabilizing effect of adding a Pt_3Cu unit, the dissociation energy, here named as D_{0,Pt_3Cu}, was calculated. These dissociation energies are calculated with the following equations:

$$D_{0,at} = \frac{1}{4n}\left(E_{(Pt_3Cu)_n} - nE_{Cu} - 3nE_{Pt} - ZPE\right) \quad (1)$$

$$D_{0,Pt_3Cu} = E_{(Pt_3Cu)_n} - nE_{Pt_3Cu} \quad (2)$$

where $E_{(Pt_3Cu)_n}$ denotes the total energy of the cluster of n units, E_{Cu} and E_{Pt} are the atomic energy of Cu and Pt respectively, and ZPE is the zero-point energy of the Pt_3Cu_n cluster, obtained in the calculation of the frequency normal modes.

In Table 1 are reported (in eV) the calculated values of the $D_{0,at}$ and the D_{0,Pt_3Cu} for the $(Pt_3Cu)_n$ $n = 10, 11$ clusters. As we can see from this table, both calculated dissociation energies show a tendency to increase as more Pt_3Cu units are added to the system. This result is in concordance with our previous findings about the smaller size clusters, being the clusters more stable as the system size increases [24].

Analyzing in detail the electron spin multiplicities of the $(Pt_3Cu)_n$, $n = 1–11$ clusters from Fig. 3, we observe that in general the clusters prefer low spin multiplicities. We notice that the most common spin multiplicity found is triplet for the clusters with n even, and the typical spin multiplicities of clusters with n odd is doublet or quartet. More information concerning the electron spin multiplicity can be obtained by the magnetic moment per atom (MMA). Therefore, in Table 1 the MMA values (in μ_B) calculated for the $(Pt_3Cu)_n$, $n = 10, 11$ clusters are also reported. As we can see the MMA value of the Pt_3Cu_{11} cluster is about 0.06 μ_B, i.e., almost twice bigger than the Pt_3Cu_{10} cluster. This new result, together with the results obtained in our previous study of the smaller cluster sizes, shows a clear tendency of the bigger Pt_3Cu_n-type clusters to increase the MMA as the system size grows [24].

To understand where in these nanoclusters the electron spin multiplicity is concentrated, the electron spin density of the $(Pt_3Cu)_n$ $n = 10, 11$ clusters in their cationic, neutral and anionic species was plotted and the obtained results are presented in Fig. 4. In this figure the spin multiplicities of all species is also indicated to the reader. For the $(Pt_3Cu)_{10}$ clusters, as Fig. 4 shows, the spin density distribution is most concentrated on Pt atoms located opposite to the apex of the structure with "missing atoms". Both ionic structures have a spin multiplicity of quartet, whereas, as it was already

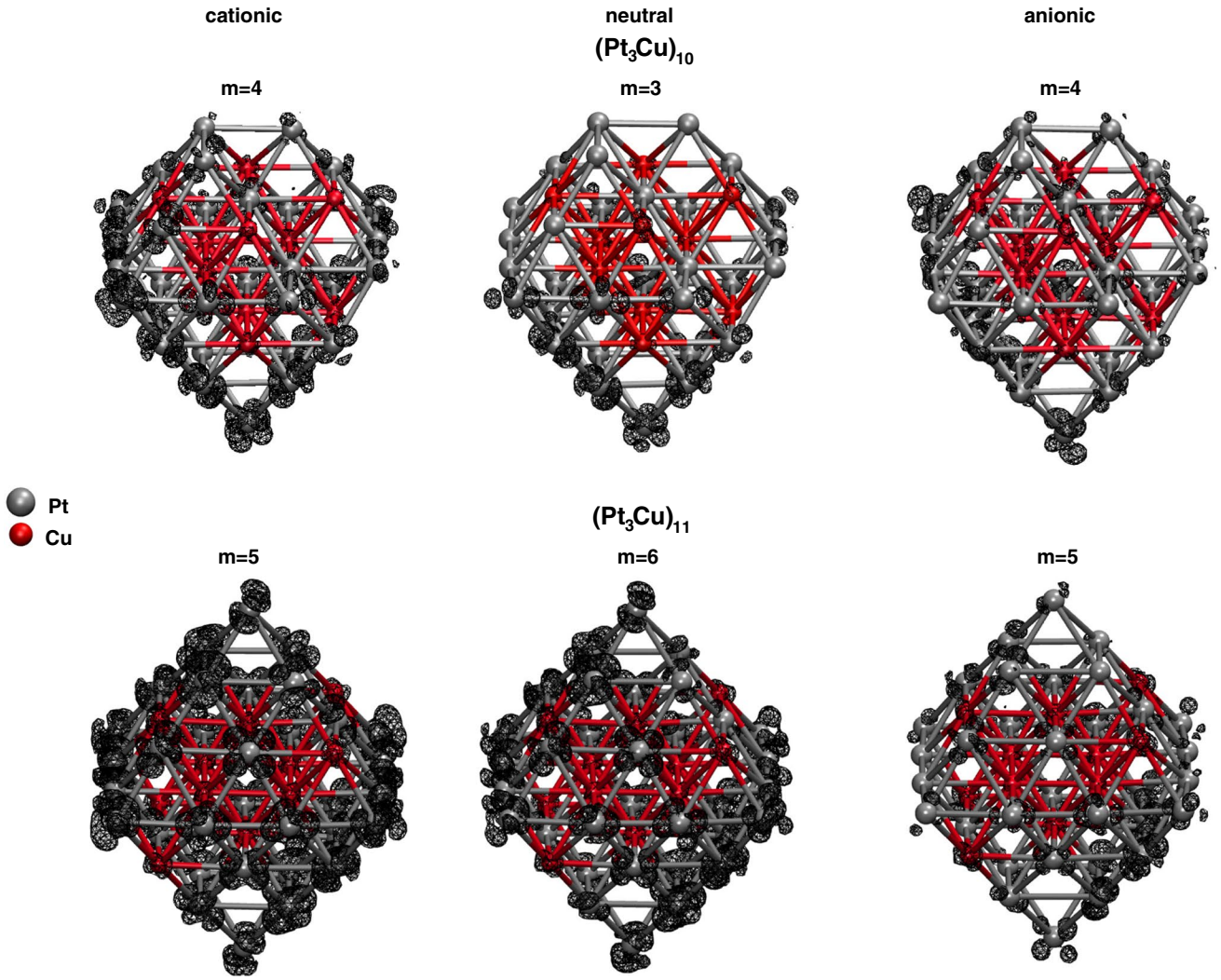

Fig. 4 Plots of electron spin density of the $(Pt_3Cu)_n$ nanoclusters with $n = 10$–11 in their cationic, anionic and neutral ground state structures

Table 1 Calculated dissociation energy ($D_{0,At}$ and D_{0,Pt_3Cu}) and MMA for the $(Pt_3Cu)_n n = 10, 11$ clusters

n	$D_{0,At}$ (eV)	D_{0,Pt_3Cu} (eV)	MMA (μ_B)
10	3.63	5.73	0.0707
11	3.68	5.95	0.1345

discussed, the neutral specie has triplet spin multiplicity. Different to the $Pt_{30}Cu_{10}$ cluster, all species of the $(Pt_3Cu)_{11}$ cluster present a more homogeneous spin density distribution on the Pt-rich regions of the system (see Fig. 4). The most stable structures of the ionic species of this nanocluster are both found on the quintet PES. We notice that in general there is no spin density allocated on the Cu atoms of these nanoclusters formed with either 10 or 11 Pt_3Cu units.

To have a better understanding of the structure geometry in relation with the atomic distribution in all cluster species, the average bond length (ABL) of the Pt–Pt, Pt–Cu and Cu–Cu bonds of the $(Pt_3Cu)_n$ $n = 10, 11$ clusters, along with their approximate cluster size were calculated in the cationic, neutral and anionic states. The obtained results are listed (in Å) in Table 2. We notice that there is almost no difference in all types of calculated ABL between the different states of each cluster. From this result we can conclude that the charge does not affect significantly a special type of bond. Also, in the case of the approximate cluster sizes, as we can see from Table 2, the obtained results are very similar. The obtained results show that for the Pt–Cu and the Pt–Pt ABL the obtained values are almost the same for both cluster sizes in all states, lying all results in a range of only 0.01 Å. However, the most significant difference between the clusters is obtained for the Cu–Cu ABL, in which a difference of about 0.04 Å can be noticed between the $(Pt_3Cu)_{10}$ and the $(Pt_3Cu)_{11}$ nanoclusters (Table 2). This result can be explained considering that in the $(Pt_3Cu)_{11}$ nanocluster the

Table 2 Calculated ABL for Cu–Cu, Cu–Pt and Pt–Pt bond distances and the approximate system size for the $(Pt_3Cu)_n$ $n = 10$–11 clusters in their anionic (a), neutral (n) and cationic (c) states

n	state	Cu–Cu	Pt–Cu	Pt–Pt	Approximate size
	a	2.69	2.71	2.70	11.33
10	n	2.70	2.71	2.70	11.37
	c	2.70	2.71	2.69	11.37
	a	2.66	2.72	2.70	11.30
11	n	2.66	2.72	2.70	11.31
	c	2.66	2.72	2.70	11.32

All values are given in (in Å). See text for details

Table 3 Vertical and adiabatic IP, EA and Δ for the $(Pt_3Cu)_n$, $n = 10, 11$ clusters

n	IP	EA	Δ
Vertical			
10	6.38	3.84	2.54
11	6.43	3.92	2.51
Adiabatic			
10	6.37	3.82	2.56
11	6.42	3.97	2.45

All values are in eV. See text for details

Cu atoms form a core structure, in which six Cu atoms build a smaller octahedron inside the system. The existence of this core structure can also explain the diminishing in the approximate size noticed between these nanoclusters, being the $(Pt_3Cu)_{11}$ nanocluster smaller in size for all calculated states with respect the $(Pt_3Cu)_{10}$ nanocluster species.

3.2 Energetic properties

The vertical and adiabatic ionization potential (IP), the vertical and adiabatic electron affinity (EA), as well as the difference between the calculated IP and EA, denoted here as Δ, were calculated for the $(Pt_3Cu)_n$ $n = 10, 11$ nanoclusters. In Table 3 the obtained results are reported in eV.

As Table 3 shows the vertical and adiabatic properties are quite similar between each other, being the largest differences within a window of only 0.05 eV. This result is on line with the obtained ABL results for the ionic and neutral species and indicates that the change in geometry and energy of the optimized ionic structures is not very significant. This finding should be taken into account if one aims to extend this type of investigation to larger clusters in order to save computational time. We notice that the calculated IP and EA values slightly increase as the nanocluster size grows. To gain more insight about the nature of these nanoparticles, the difference between the computed IPs and EAs was calculated. This property is an approximation for the HOMO-LUMO gap of the clusters. As we see from Table 3, the calculated Δ decreases as the cluster size increases. This behavior is expected because in the bulk limit, IP and EA becomes equal and Δ approaches zero, in agreement with a metallic-type system behavior.

4 Conclusions

A first-principle ADFT study of $(Pt_3Cu)_n$ $n = 10, 11$ nanoclusters was performed. To investigate these nanoparticles, Born-Oppenheimer Molecular Dynamics (BOMD) trajectories at different temperatures were generated for each system size. Several dozens of isomers in different spin multiplicities were taken as initial structures for successive geometry optimization along these BOMD trajectories. In this way a more detailed exploration of the potential energy surfaces of these nanoclusters was performed. All geometry optimization were performed without any restrictions to find the most stable structure of both studied nanoclusters considering their neutral, anionic and cationic species. The optimized structures were characterized by frequency analysis calculations to assure their character as minimum on the corresponding potential energy surfaces. This is the first ab-initio-based work for which nanometric sizes structures of this type of systems were fully optimized.

This study was performed to answer the question if either octahedra or twinned octaedra-type structures are preferred for the most stable structures of large Pt_3Cu-based clusters. The results of the obtained most stable structures, of the harmonic frequencies, of the analysis of bond lengths, the computed electron spin density and energy properties such as ionization potential, electronic affinity and their differences were presented. An important finding of this study is that the most stable structure of the largest investigated Pt_3Cu nanoparticle (whose size is about 1.15 nm!) is the simple octahedron.

However, since as we have seen in the smaller cluster sizes, the creation of single octahedron structures involves the formation of twinned octahedra, the experimental creation of twinned octahedra nanoparticles of this type could be possible using correct reagents. It has been already observed in experimental works that a simple Cu salt precursor change would affect the morphology of nanoparticles [7]. To the best of our knowledge to the date, no information of synthesized twinned octahedra nanoparticles of Pt_3Cu of a few nanometers size are available. It would be an interesting perspective of this investigation to continue exploring this alloy in the synthetic area.

Supplementary Information The online version contains supplementary material available at https://doi.org/10.1007/s00214-023-02963-4.

Acknowledgements C.D. Galindo Uribe acknowledges CONACyT for the doctoral fellowship 864427. The financial support of the CB-252658 project is acknowledged.

Declarations

Conflicts of interest There are no conflict of interest to declare.

References

1. Khan MAR, Al Mamun MS, Ara MH (2021) Review on platinum nanoparticles: synthesis, characterization, and applications. Microchem J 171:106840
2. Roduner E (2006) Nanoscopic materials size-dependent phenomena. RSC Publishing, Cambridge
3. Seh ZW, Kibsgaard J, Dickens CF, Chorkendorff IB, Nørskov JK, Jaramillo TF (2017) Combining theory and experiment in electrocatalysis: insights into materials design. Science 355:6321
4. Cruz-Martínez H, Tellez-Cruz MM, Guerrero-Gutiérrez OX, Ramírez-Herrera CA, Salinas-Juárez MG, Velázquez-Osorio A, Solorza-Feria O (2019) Mexican contributions for the improvement of electrocatalytic properties for the oxygen reduction reaction in PEM fuel cells. Int J Hydr Ener 44:12477–12491
5. Nørskov JK, Rossmeisl J, Logadottir A, Lindqvist LRKJ, Kitchin JR, Bligaard T, Jonsson H (2004) Origin of the overpotential for oxygen reduction at a fuel-cell cathode. J Phys Chem B 108:17886–17892
6. Oezaslan M, Hasché F, Strasser P (2012) *PtCu*$_3$, *PtCu* and Pt_3Cu alloy nanoparticle electrocatalysts for oxygen reduction reaction in alkaline and acidic media. J Electrochem Soc 159:B444
7. Sun X, Jiang K, Zhang N, Guo S, Huang X (2015) Crystalline control of 111 bounded Pt_3Cu nanocrystals: multiply-twinned Pt_3Cu icosahedra with enhanced electrocatalytic properties. ACS Nano 9:7634–7640
8. Wu Z, Dang D, Tian X (2019) Designing robust support for Pt alloy nanoframes with durable oxygen reduction reaction activity. ACS Appl Mater Interfaces 11:9117–9124
9. Wang X, Li Z, Qu Y, Yuan T, Wang W, Wu Y, Li Y (2019) Review of metal catalysts for oxygen reduction reaction: from nanoscale engineering to atomic design. Chem 5:1486–1511
10. Kuang Y, Cai Z, Zhang Y, He D, Yan X, Bi Y, Sun X (2014) Ultrathin dendritic Pt_3Cu triangular pyramid caps with enhanced electrocatalytic activity. ACS Appl Mater Interfaces 6:17748–17752
11. Pham HQ, Huynh TT (2021) Platinum-copper bimetallic nanodendritic electrocatalyst on a TiO_2-based support for methanol oxidation in alkaline fuel cells. ACS Appl Nano Mater 4:4983–4993
12. Magalhães MM, Gomes JF, Tremiliosi-Filho G, de Figueiredo PB, de Lima RB, Colmati F (2021) Ethanol electro-oxidation on carbon-supported Pt_3Sn/C, Pt_3Cu/C and $PtSnCu/C$ catalysts: CV and in situ FTIR study. J Appl Electrochem 51:173–181
13. Song P, Lei Y, Hu X, Wang C, Wang J, Tang Y (2020) Rapid one-step synthesis of carbon-supported platinum–copper nanoparticles with enhanced electrocatalytic activity via microwave-assisted heating. J Colloid Interface Sci 574:421–429
14. Chaves AS, Rondina GG, Piotrowski MJ, Da Silva JL (2015) Structural formation of binary PtCu clusters: a density functional theory investigation. Comput Mater Sci 98:278–286
15. Chaves AS, Piotrowski MJ, Guedes-Sobrinho D, Da Silva JL (2015) Theoretical investigation of the adsorption properties of CO, NO, and OH on monometallic and bimetallic 13-atom clusters: the example of Cu_{13}, Pt_7Cu_6, and Pt_{13}. J Phys Chem A 119:11565–11573
16. Gálvez-González LE, Juárez-Sánchez JO, Pacheco-Contreras R, Garzón IL, Paz-Borbón LO, Posada-Amarillas A (2018) CO_2 adsorption on gas-phase $Cu_{4-x}Pt_x$ (x=0-4) clusters: a DFT study. Phys Chem Chem Phys 20:17071–17080
17. Nilekar AU, Mavrikakis M (2008) Improved oxygen reduction reactivity of platinum monolayers on transition metal surfaces. Surf Sci 602:89–94
18. Yang L, Vukmirovic MB, Su D, Sasaki K, Herron JA, Mavrikakis M, Liao S, Adzic RR (2013) Tuning the catalytic activity of Ru@Pt core-shell nanoparticles for the oxygen reduction reaction by varying the shell thickness. J Phys Chem C 117:1748–1753
19. Stamenkovic VR, Fowler B, Mun BS, Wang G, Ross PN, Lucas CA, Marković NM (2007) Improved oxygen reduction activity on Pt3Ni(111) via increased surface site availability. Science 315:493–497
20. Calaminici P, Alvarez-Ibarra A, Cruz-Olvera D, Dominguez-Soria V, Flores-Moreno R, Gamboa GU, Geudtner G, Goursot A, Mejia-Rodriguez D, Salahub DR, Zuniga-Gutierrez B, Köster AM (2017). In: Leszczynski J et al (eds) Handbook of computational chemistry Part II: applications of computational methods to model systems, 2nd edn. Springer, Cham
21. Cruz-Martínez H, Rojas-Chávez H, Matadamas-Ortiz PT, Ortiz-Herrera JC, López-Chávez E, Solorza-Feria O, Medina DI (2021) Electrocatalysis of oxygen reduction on CoNi-decorated-Pt nanoparticles: a theoretical and experimental study. Mater Today Phys 19:100406
22. Flores-Rojas E, Cruz-Martínez H, Rojas-Chávez H, Tellez-Cruz MM, Reyes-Rodríguez JL, Cabañas-Moreno JL, Solorza-Feria O (2018) A combined DFT and experimental investigation of Pt-wrapped CoNi nanoparticles for the oxygen reduction reaction. Electrocatalysis 9:662–672
23. Flores-Rojas E, Cruz-Martínez H, Tellez-Cruz MM, Pérez-Robles JF, Leyva-Ramírez MA, Calaminici P, Solorza-Feria O (2016) Electrocatalysis of oxygen reduction on CoNi-decorated-Pt nanoparticles: a theoretical and experimental study. Int J Hydr Ener 41:23301–23311
24. Galindo-Uribe CD, Calaminici P, Cruz-Martínez H, Cruz-Olvera D, Solorza-Feria O (2021) First-principle study of the structures, growth pattern, and properties of $(Pt_3Cu)_n$, n=1-9, clusters. J Chem Phys 154:154302
25. Köster AM, Geudtner G, Alvarez-Ibarra A, Calaminici P, Casida ME, Carmona-Espindola J, Dominguez VD, Flores-Moreno R, Gamboa GU, Goursot A, Heine T, Ipatov A, de la Lande A, Janetzko F, del Campo JM, Mejia-Rodriguez D, Reveles JU, Vasquez-Perez J, Vela A, Zuniga-Gutierrez B, Salahub DR (2018) deMon2k, Version 6. The deMon developers, Cinvestav, Mexico City
26. Köster AM, Flores-Moreno R, Reveles JU (2004) Efficient and reliable numerical integration of exchange-correlation energies and potentials. J Chem Phys 121:681
27. Zhang Y, Yang W (1998) Comment on "Generalized gradient approximation made simple''. Phys Rev Lett 80:890
28. Perdew JP, Burke K, Ernzerhof M (1996) Generalized gradient approximation made simple. Phys Rev Lett 77:3865
29. Calaminici P, Janetzko F, Köster AM, Mejia-Olvera R, Zuniga-Gutierrez B (2007) Density functional theory optimized basis sets for gradient corrected functionals: 3d transition metal systems. J Chem Phys 126:044108
30. Hay PJ, Wadt WR (1985) Ab initio effective core potentials for molecular calculations. Potentials for K to Au including the outermost core orbitals. J Chem Phys 82:299–310
31. Schuchardt KL, Didier BT, Elsethagen T, Sun L, Gurumoorthi V, Chase J, Windus TL et al (2007) Basis set exchange: a community database for computational sciences. J Chem Inf Model 47:1045–1052

32. Martins LSC, Jorge FE, Machado SF (2015) All-electron segmented contraction basis sets of triple zeta valence quality for the fifth-row elements. Mol Phys 113:3578–3586
33. Humphrey W, Dalke A, Schulten K (1996) VMD: visual molecular dynamics. J Mol Graph 14:33–38
34. Nosé S (1984) A unified formulation of the constant temperature molecular dynamics methods. J Chem Phys 81:511–519
35. Martyna GJ, Klein ML, Tuckerman M (1992) Nosé–Hoover chains: the canonical ensemble via continuous dynamics. J Chem Phys 97:2635–2643
36. Delgado-Venegas RI, Mejía-Rodríguez D, Flores-Moreno R, Calaminici P, Köster AM (2016) Analytic second derivatives from auxiliary density perturbation theory. J Chem Phys 145:224103